EVALUATION OF SEMI-AUTOMATED TARGET EXTRACTION METHODS FOR DIGITAL CLOSE-RANGE PHOTOGRAMMETRY

Sagar Deshpande, Ferris State University

Abstract

Digital close-range photogrammetry is used for 3D reconstructions in many industries such as automobile and aircraft manufacturing, shipbuilding, and large-scale engineering construction. It commonly uses artificial targets to precisely locate a particular object on overlapping images. Image coordinates of the targets can be extracted manually or by implementing automated image processing algorithms. In this study, the author evaluated five target identification methods using a test field. Overlapping images were acquired of several targets placed on the test field using an off-the-shelf digital camera. These methods were then used to extract sub-pixel image coordinates of these artificial targets. Accuracy was evaluated based on 3D coordinates of these targets that were computed using the direct linear transform method. Based on the results, it was found that, among the five methods, the interpolation method produced the best results.

Introduction

In the manufacturing industry, high quality is achieved by fabricating parts or components as close to design specs as possible. Traditional methods can be used to make several measurements on a component to create a three-dimensional (3D) model, but they are time consuming and provide measurements at only a few locations. Similarly, advanced terrestrial scanners can also provide accurate 3D models. But, when compared to photogrammetry, they cannot be used in certain situations, due to high data acquisition times. On the other hand, digital close-range photogrammetry (DCRP) can be used to make several measurements on the object by capturing images from different locations. With the development in camera sensor technology, the quality and affordability of digital cameras have increased, resulting in increased use of close-range mapping applications. Therefore, DCRP systems, so-called vision metrology (VM) systems, have gained a footing for high-precision measurements on the commercial market.

Artificial targets are used in aerial photogrammetry and in close-range photogrammetry to facilitate precise photographic measurements. They are designed based on field conditions and camera properties. To achieve high photogrammetric accuracy, it is necessary to precisely identify the target's center. In this paper, five methods for extracting a target's center are presented. These methods use the digital number (DN) variations of targets on digital images. A close range photogrammetry setup was used to evaluate the accuracy achieved by these methods. Three sets of control targets (CTs) were used for camera calibration, using the direct linear transform (DLT) method. Thirty measure targets (MTs) were used for accuracy assessment by calculating standard errors.

Background Review

DCRP has been used in several applications for 3D reconstruction [1-7]. It is mainly used in mapping objects with limited time availability because of quick data acquisition capability [2-3, 8]. One of the primary, but tedious, tasks in photogrammetry is to identify common points on multiple overlapping images. Issues such as variable surface reflectivity, non-ideal illumination, and occlusion could make this task more complicated. Various image matching algorithms can be used to automate and expedite point-based matching. Generally, targets are used to facilitate and expedite matching. Targets can be classified as natural and artificial [4]. Natural targets are points or locations on an image with unique image properties, such as the corner of a road intersection. Artificial targets, which are typically symmetric in shape, are printed on a reflective material so that they can be easily identified in on an image [5], due to high contrast and shape properties.

Several researchers have experimented using of different target shapes such as circular [2, 4, 9-15], rectangular [2, 9], dots [3, 16], or other symmetric patterns [3, 4, 17]. Several researchers have implemented methods to extract the center of targets, depending on the shape of the target. A method to extract coordinates of crosses from analog continuous tone pictures using CCD (charged coupled device) cameras and comparing the mean error in image plane coordinates, was described by Jachimski and Trocha [18]. Based on spatial resolution, quantization accuracy, and noise, West and Clarke [19] experimentally analyzed and assessed four tech-

niques—centroid, weighted centroid, vernier, and interpolation. Use of a chess-board pattern is also a common target [20]. A chess-board pattern is extracted to the sub-pixel level by calculating the center of gravity of areas formed by connecting corners of high correlation [20]. Shortis et al. [17] presented coded targets that employed polar coordinate transformation and segment matching to automatically recognize and identify targets in digital images. Perez et al. [21] used a grid pattern provided by Photomodeler software for camera calibration. This software was designed to extract the predefined grid pattern for photogrammetric calculations.

Use of coded targets has been reported by several researchers to automatically label the identified targets [12] [11-15, 22]. They expedited the target matching process and removed error caused by human misinterpretation. Most of these methods are based on modeling the shape of the target on the image. Circular and square targets with thin cross-hairs at their centers were used. Five different semi-automatic methods, which were specifically developed for this target pattern, were used to extract the targets.

Methodology

Figure 1 shows that the methodology adopted for this study was divided into three stages: data acquisition, data reduction, and data presentation [5]. It should be noted that the overall accuracy of a photogrammetric system depends on the accuracy of target extraction. Therefore, this paper includes only detailed descriptions of the five methods.

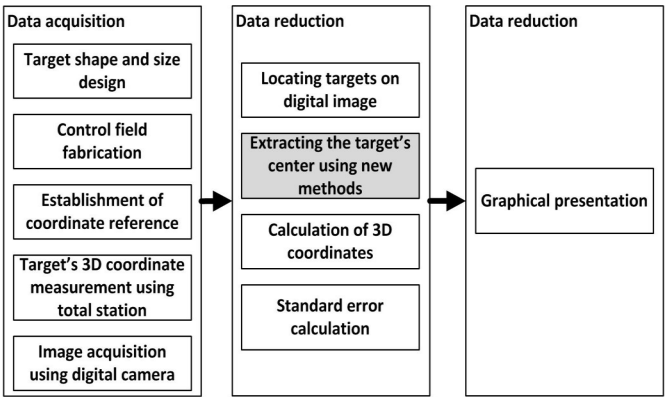

Figure 1. Methodology Adopted for This Study

Data Acquisition

In this stage, a 3D test field with dimensions of 1.0m (length), 0.6m (width), and 1.5m (height) was fabricated in the laboratory (see Figure 2).

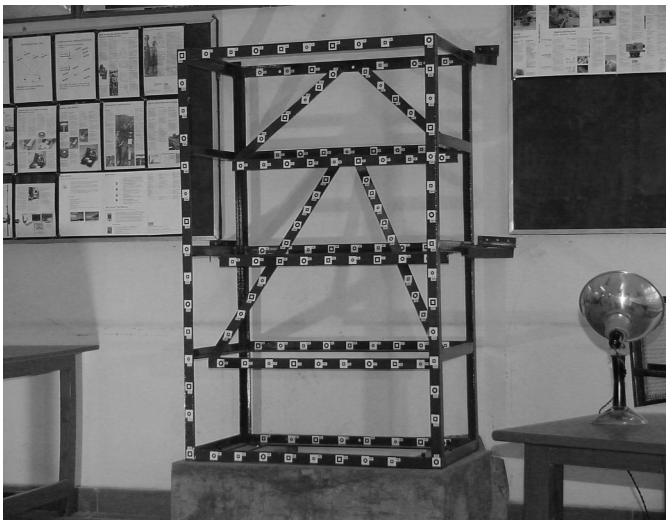

Figure 2. Fabricated Test Field in the Laboratory and Location of the Targets

Based on factors such as the nominal focal length of the camera (12.5 mm), the size of the CCD elements (6.3 microns), the object-to-camera distance (6.2 m), and the number of pixels that form a target on an image (12 to 15 pixels), three different sizes of targets were used: l = 12 mm, 16 mm, and 20 mm. These targets were printed on high-quality photographic paper, using a laser plotter and were fixed on the test field. The thickness, t, of the target was designed to be equal to 3 mm (see Figure 3).

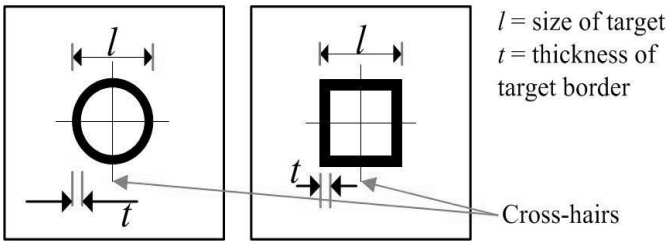

Figure 3. Shape and Dimensions of the Targets

The 3D coordinates of these targets were required for camera calibration and accuracy assessment. Therefore, the next step was to measure the coordinates of these targets. Figure 4(a) shows how a coordinate reference was established with its origin at point S_1. The 3D coordinates of point S_1 was assumed to be 100m, 100m, and 100m in the X, Y, and Z directions, respectively. Figure 4(b) shows that the X axis passes through station point S_2, the Y axis is parallel to the vertical plumb direction, and the Z axis is perpendicular to both X and Y directions. Vertical and horizontal angles to each target were measured from stations S_1 and S_2, using Trimble's total station (model SR5600 DR+200). This instrument has an angular precision of ±1 second. Crosshairs printed on the targets were used to make accurate

angular measurements. Distance B between stations S_1 and S_2 was measured using fiberglass tape and a diagonal scale. Using the horizontal and vertical angular measurements from stations S_1 and S_2, and the distance B, 3D coordinates of all the targets were calculated using trigonometric relationships.

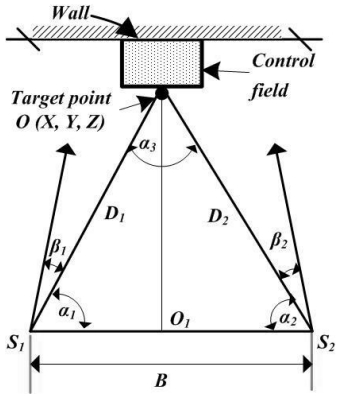

(a) Top View of the Two Points S_1 and S_2 and the Test Field

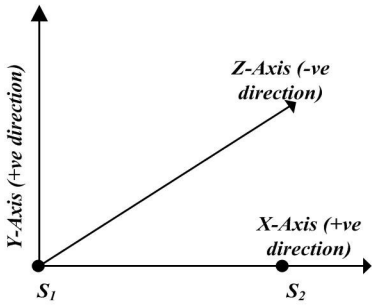

(b) 3D View of the Coordinate System Located at Station S_1

Figure 4. Schematic Representation of the 3D Coordinate System

Figure 5 shows how the images of the test field were then acquired from approximately 6.2m using an off-the-shelf digital camera (Sony MVC-FD95, a 2-megapixel camera). The field of view of cameras was kept such that the axes of the cameras converged onto the test field. These images were transferred to a computer to perform the steps in the data-reduction stage.

Data Reduction

Extraction of the image coordinates of the targets, calculation of object-space coordinates using image coordinates, and calculation of the standard error of the computed targets were the steps in this stage. The target-extraction step consisted of two sub-steps: to locate the targets on the digital image and to extract the center of each located target.

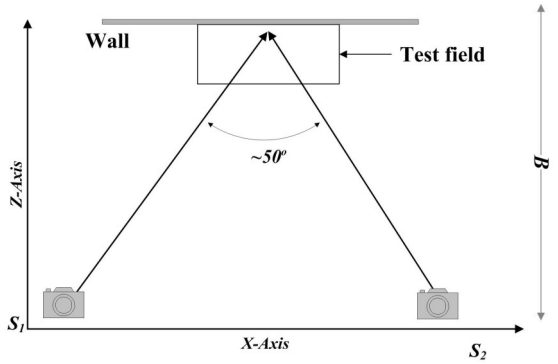

Figure 5. Top View of the Camera Positions and Test Field during Image Capture

In the first sub-step, edge detection [23] was performed on the original image [see Figure 6(a)] to create a binary image [see Figure 6(b)]. This binary image consisted of 0s (black color) at edge locations on the image and 1s (white color) for the rest of the image. A sample target was then manually defined using a mouse pointer, by specifying a representative target on a binary image [see Figure 6(b)]. This target was used for template matching, using cross-correlation [24] to locate other similar targets on the image. Since the entire test field had targets of different sizes and shapes, this step was repeated (usually 4-5 times) until all of the targets used in this study were located.

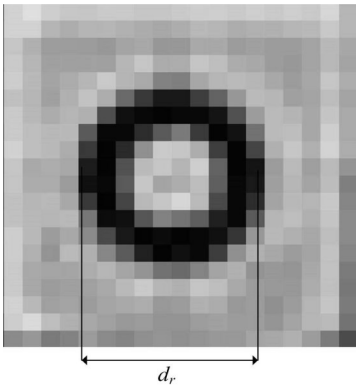

(a) Target Formed on the Original Image

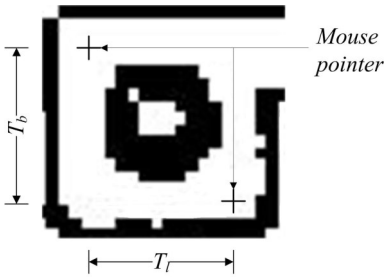

(b) Target Formed on the Binary Image after Edge Detection

Figure 6. Sample Target

In the second sub-step, each located target was processed to find the central area of the target. In this process, the original image and the binary image were used interchangeably. Figure 7 shows the step-by-step procedure, which is explained below:

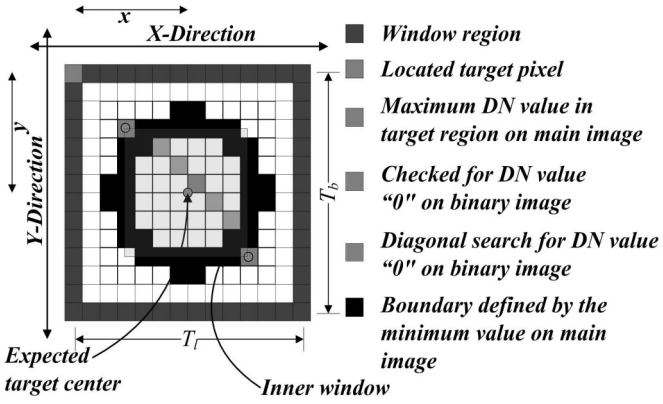

Figure 7. A Schematic Target Showing Different Features Used for Target Extraction

1. A window equal to the size of a manually specified target was placed around a located target. A diagonal search was performed on the binary image from the upper left and lower right corners of the window to locate the "0" DN value. An inner window was obtained by connecting the two "0" DN value locations.
2. As the area within this region contained only the target's ring and the inner region, the maximum DN value within the inner window was identified using the original image. This search would point to a pixel location in the inner region of the target.
3. A "0" DN value was searched on the binary image up to a distance of half of the sample target ($T_b/2$ or $T_l/2$) diagonally away from the maximum DN value location. All rows and columns containing the pixel along the diagonal direction between the "0" DN value locations were used for extracting the target's center.
4. For each row and column, the border pixels were identified on the original image by searching for the minimum DN value, up to a distance of half of the sample target ($T_b/2$ or $T_l/2$) on either side of the diagonal pixel.

After locating the inner extents of the target, all rows and columns within similar boundaries were used for identification of the target's center. The following methods were developed to locate a target's center to the sub-pixel level.

Method 1: Interpolation

The interpolation method was modified, based on the interpolation method by Jachimski & Trocha [18]. Compared to their method, the modified method used fewer points along the profile. DN values in each row and column of a target, when plotted, resembled a bell-shaped curve. Figure 8 shows a sample profile in which the lower DN values at 4 and 13 locations along the horizontal axis are represented by the black border of the target, while small depressions in the central portion (at position 9) of profile was due to the crosshairs.

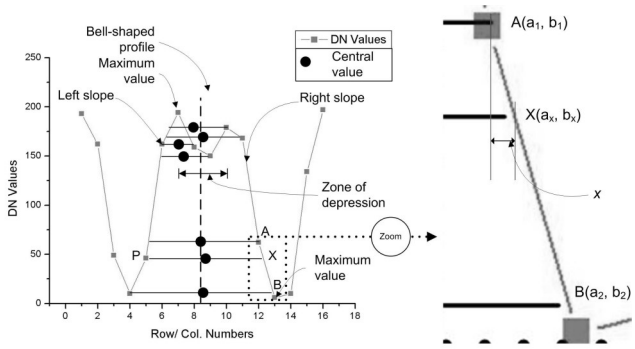

Figure 8. Profile of the DN Values in the Target Showing the Interpolation Method

To calculate the center, each point on the profile was processed individually. Point P in Figure 8 is used as an example to explain the process. It can be noted that the target's approximate center is half way between points P and X. Point X, which is equal to the DN value at P, represents an interpolated location on the right profile between points A and B. Therefore, distance PX is equal to the sum of distances PA and AX, measured horizontally. Points P and A are located at 5 and 12, respectively. Using the gradient between points A and B, distance $AX = x$ can be calculated. Therefore, distance PX can be determined using Equation (1):

$$PX = 12 - 5 + x \tag{1}$$

The center was considered to be located at a distance of $PX/2$, which is shown as the "Central value" in Figure 8. Several such center locations were calculated for every DN value in every row within the target's boundary. The averaging and thresholding process was implemented on these calculated center locations to obtain the target's center coordinates along the row. This procedure was also implemented for all DN values along the column within the target's boundary to obtain the target's center coordinates along the column.

Method 2: Cubic Spline

This method was adapted using the polynomial line-fitting approach [18] and utilized the cubic spline interpolation to estimate the center of the target along a row or column profile. The cubic spline function is a third-order curve em-

ployed to connect each pair of data points so that the connections between adjacent cubic equations are smooth. Therefore, this method was used to find the target's center. Figure 9 shows the profile of DN values within the target for a typical row. In this figure, a dip in DN value can be observed between pixel locations 3 and 7. This was due to the crosshair located at the center of target. Therefore, based on observation of the profiles, the middle third of the pixel values were excluded for this method. Figure 9 also shows how a cubic spline equation [25] was fitted to the remaining DN values. The location at which this cubic spline attained the maximum value was considered as the center for a particular row. Therefore, one center value was calculated for every row within a target. The averaging and thresholding process was implemented on these calculated center locations to obtain the target's center coordinates along the row.

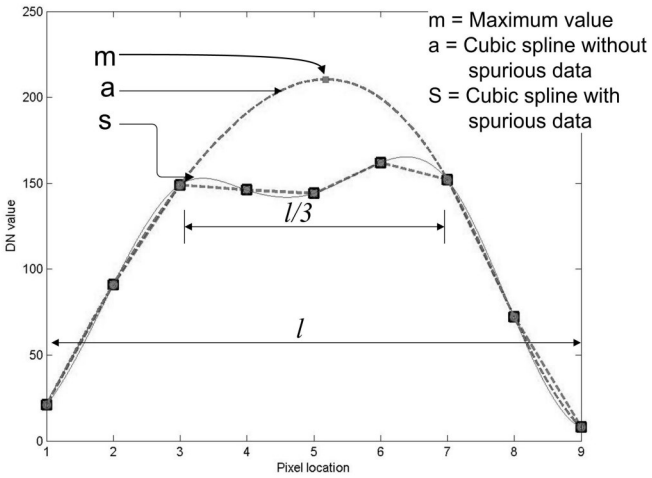

Figure 9. Graphical Representation of the Cubic Spline Method

This procedure was also implemented for all columns within a target's boundary to obtain the target's center coordinates along the column.

Method 3: Moment of DN Values

This new method utilized a principle from engineering statics. In Statics, moment of a force is a measure of its tendency to cause a body to rotate about a specific point or axis. In order to keep a body stable, the magnitude of positive and negative moments should be equal. This principle was used to determine the target's center. This method was implemented for all of the pixels in the horizontal direction within the target's boundary. The left-most column containing the border pixel was considered as an axis about which positive and negative moments were calculated [see Figure 10(b)]. Each row in a target's boundary was assumed to be a horizontal beam with the DN values as forces acting vertically downward [see Figure 10(a)].

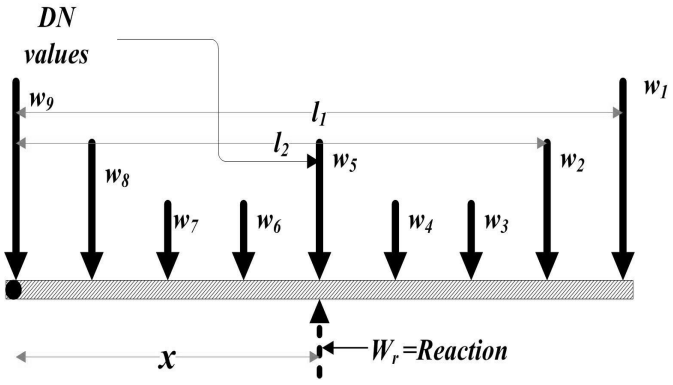

(a) DN Values Acting on a Beam

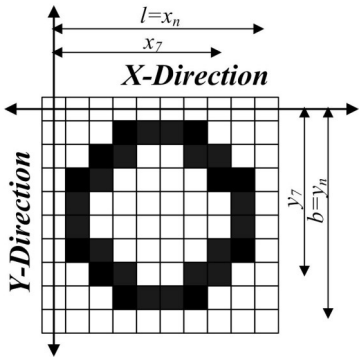

(b) Moments Calculated Along the X and Y Axes

Figure 10. Moment-of-Area Method

Figure 10(a) shows the axis as pivot point; *W's* represent the *n* number of DN values within the target's border; *l's* represent the distance to these pixels from the axis; and W_r, which is vertical, represents a reaction force equal to the sum of all *W's*. By equating the positive and negative moments, the value of *x* was calculated using Equation (2):

$$x = \frac{\sum_{i=1}^{n} W_i l_i}{\sum_{i=1}^{n} W_i} \tag{2}$$

Similar calculations were implemented in the column direction to calculate the target's center.

Method 4: Average Number of Pixels below Threshold

This method was adapted based on similar center-of-gravity methods proposed by other researchers [14, 26]. In this method, pixels in a target region, which have DN values below a certain threshold, were used to calculate the center of the target.

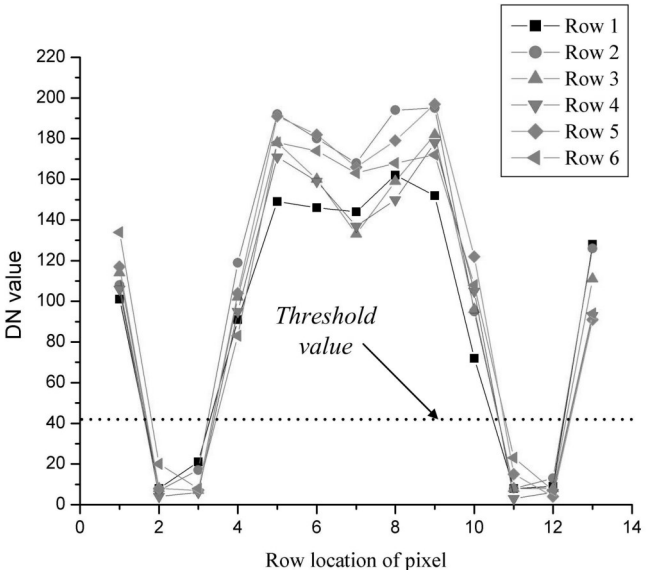

Figure 11. Implementation of the Average-Below-Threshold Method

Figure 11 shows typical DN values profiles along the rows within a target. Based on the observation that the pixels along the target's black border had DN values below 40, a minimum DN threshold value of +40 was adopted to shortlist the pixels that formed the target's border. The average of the row and column numbers for shortlisted pixel locations was calculated using Equation (3):

$$x = \frac{\sum_{i=1}^{n} C_i}{n} \quad y = \frac{\sum_{i=1}^{n} R_i}{n} \tag{3}$$

where, x and y are the image coordinates of the target's center; C is the column number of shortlisted pixels; R is the row number of shortlisted pixels; and, n is the number of shortlisted pixels.

The calculated x and y values were considered as the target's center image coordinates along the rows and columns, respectively.

Method 5: Weighted Average-Below-Threshold

This method was an extension of the aforementioned method. In this method, weighted average values of the pixel locations below the threshold value were calculated using Equation (4):

$$x = \frac{\sum_{i=1}^{n} W_i C_i}{\sum_{i=1}^{n} W_i} \quad y = \frac{\sum_{i=1}^{n} W_i R_i}{\sum_{i=1}^{n} W_i} \tag{4}$$

where, W represents the DN values in n number of pixels.

The calculated x and y values were considered as the target's center image coordinates along the rows and columns, respectively. In the interpolation and spline methods, several center locations were calculated in row and column directions for a target. The averaging and thresholding process was used to calculate the average value for the target's center in the horizontal and vertical directions. This method was modified based on the work by Jachimski and Trocha [18]. Figure 12 shows the method used to calculate the center.

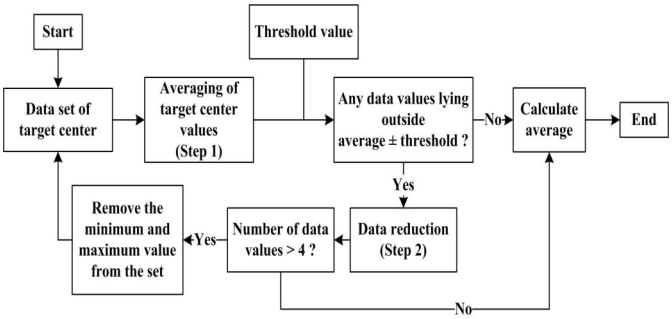

Figure 12. Flowchart Describing the Averaging and Thresholding Method

In the first step, the average (μ) of the set of multiple center coordinates along the rows was calculated. A check was performed to find values in the set that were greater than μ ± the threshold. If any values were greater than μ ± the threshold then the minimum and maximum values were removed from the set. This process was repeated until either the number of coordinates in the set was more than four or if no values were outside the threshold criteria. The average of all the retained values in the set was considered as the center value along the rows. The same procedure was implemented along the columns. Based on experimentation, a threshold of 0.2 pixels was used in this study.

In this study, the direct linear transform (DLT) calibration approach [27] was used to calibrate the non-metric cameras and to calculate object-space coordinates. DLT establishes a direct linear relationship between coordinates of image points and the corresponding object-space coordinates. Equation (5) shows how DLT can be derived from the standard collinearity equations:

$$x = \frac{L_1 X + L_2 Y + L_3 Z + L_4}{L_9 X + L_{10} Y + L_{11} Z + 1}$$
$$y = \frac{L_5 X + L_6 Y + L_7 Z + L_8}{L_9 X + L_{10} Y + L_{11} Z + 1} \tag{5}$$

where, L_1 *to* L_{11} represent the 11 DLT parameters; X, Y, and Z are the 3D coordinates of a point; and, x and y are the image plane coordinates.

Using the five methods discussed here, image coordinates of the targets were extracted. Thirty targets were used as measuring targets (MTs), while three sets consisting of 6, 10, and 15 targets were used as control targets (CTs). Using the image coordinates and the ground 3D coordinates of CTs in the DLT method, camera calibration parameters L_1 to L_{11} were calculated. Using these parameters and the image coordinates of the 30 MTs, 3D coordinates of the MTs and their corresponding standard error were calculated. Standard variance of the adjusted quantities [28] is given by Equation (6):

$$\Sigma = \sigma_0^2 N^{-1} \tag{6}$$

where, N^{-1} is the variance-covariance matrix of the computed coordinates, shown in Equation (7), and σ_o^2 is the reference standard variance.

$$\Sigma = \begin{bmatrix} \sigma_x^2 & \sigma_{xy} & \sigma_{xz} \\ \sigma_{yx} & \sigma_y^2 & \sigma_{yz} \\ \sigma_{zx} & \sigma_{zy} & \sigma_z^2 \end{bmatrix} \tag{7}$$

The square root of the diagonal elements of the matrix in Equation (7), $\acute{o}_x^2$, $\acute{o}_y^2$, and $\acute{o}_z^2$ represent the standard error values in the X, Y, and Z directions, respectively.

Results and Discussion

Results were presented in the third stage. The average of the standard error values in the X, Y, and Z directions were computed for the 30 MTs. Results from the previous study [9] using manually picked targets were also included in the comparison with the results obtained from the five methods. These results were presented in Table 1 and were graphically represented in Figure 13. The effects of the number of control points in the X, Y, and Z directions were also studied.

The following observations were made from results of this study.

1. Performance of the interpolation method was consistently better than the remaining four methods. This may have been due to the fact that several center locations were calculated in this method to calculate the sub-pixel target's center coordinates. The lowest average standard error values in the X, Y, and Z directions were 63 µm, 27 µm, and 113 µm, respectively, for 10 CTs. The performance of the interpolation method was least affected by the variation in number of CTs.

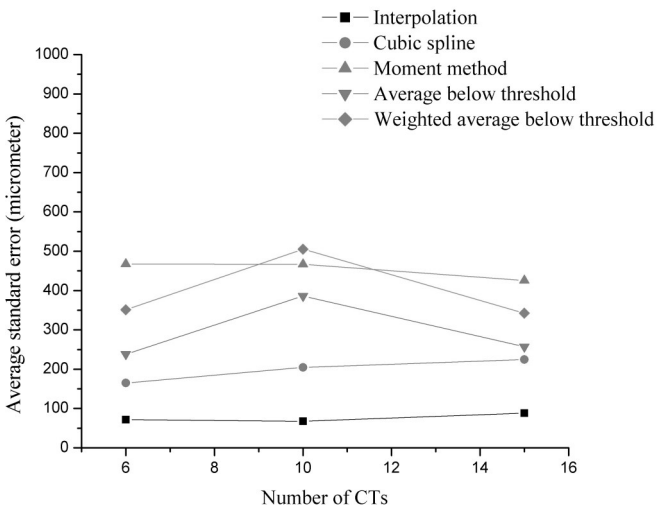

Figure 13. Graphical Representation of the Average Standard Error

Table 1. Standard Error in Micrometer (µm) for 30 MTs

Number of CTs→	6			
Method #↓	σ_x	σ_y	σ_z	σ_{Avg}
1	67	29	119	72
2	153	73	269	165
3	448	175	779	467
4	228	96	390	238
5	332	149	573	351
Manual	682	544	4309	1845
Number of CTs→	10			
Method #↓	σ_x	σ_y	σ_z	σ_{Avg}
1	63	27	113	68
2	189	85	340	205
3	433	198	769	467
4	358	158	642	386
5	464	213	838	505
Manual	492	385	3086	1321
Number of CTs→	15			
Method #↓	σ_x	σ_y	σ_z	σ_{Avg}
1	83	35	147	88
2	207	93	373	224
3	393	185	698	425
4	243	103	426	257
5	322	139	567	343
Manual	374	293	2434	1034

2. The cubic spline and the average-below-threshold methods performed similarly. The lowest error achieved by the cubic spline method were 153 µm, 73 µm, and 269 µm, in the X, Y, and Z directions, respectively, for six CTs.

3. Performance of the weighted average and the moment methods were the poorest with the lowest σ_{Avg} values of 425 µm and 343 µm, respectively. The poor performance could have been because these methods calculated a single value compared to the interpolation or cubic spline method, which calculated sets of values and used the averaging and thresholding method.
4. Maximum error was observed in the *Z* direction for all of the five methods. The σ_z values for the average-below-threshold, weighted average, and the moment method were more than 400 µm in the *Z* direction. The effect of change in number of CTs was particularly observed in the *Z* direction for all of the methods, except for the interpolation method.
5. For all of the five methods, values of σ_y were least affected by the change in number of CTs.
6. Results of all the five methods were better than that of manually selected targets. A significant improvement was observed in the *Z* direction.

Conclusion

In this paper, the author described five methods for extracting targets to the sub-pixel level using an off-the-shelf digital camera. These methods used cross-correlation to locate the targets and then perform analyses using DN values to extract targets at the sub-pixel level. Three sets of CTs were used to analyze the impact of the number of control points on the accuracy. Based on the results, it was concluded that using an off-the-shelf camera and precise methods for target extraction, micron-level accuracy can be achieved. It should also be noted that if the targets are extracted at sub-pixel level then the impact of number of CTs was not significant. Further, these methods were semi-automatically implemented. Therefore, errors caused by human misinterpretation of the target's center were removed.

References

[1] Bertin, S., Friedrich, H., Delmas, P., & Chan, E. (2013). On The Use of Close-Range Digital Stereo-Photogrammetry to Measure Gravel-Bed Topography in a Laboratory Environment. In *Proceedings of 35th IAHR Congress* (pp. 8-13).

[2] Bernat, K., & Tokarczyk, R. (2013). Automation of Measurements of Selected Targets of Photopoints in Application to Photogrammetric Reconstruction of Road Accidents. *Geomatics and Environmental Engineering*, *7*.

[3] Maas, H. G., & Hampel, U. (2006). Photogrammetric techniques in civil engineering material testing and structure monitoring. *Photogrammetric Engineering & Remote Sensing*, *72*(1), 39-45.

[4] Guarnieri, A., Vettore, A., El-Hakim, S., & Gonzo, L. (2004). Digital photogrammetry and laser scanning in cultural heritage survey. *The International Archives of the Photogrammetry, Remote Sensing and Spatial Information Sciences*, *35*, B5.

[5] Deshpande, S. (2004). *Measurement of displacement using digital close range photogrammetry (DCRP)*. (Master's thesis, IIT Kanpur, India).

[6] White, D. J., Take, W. A., Bolton, M. D., & Munachen, S. E. (2001). A deformation measurement system for geotechnical testing based on digital imaging, close-range photogrammetry, and PIV image analysis. In *Proceedings of the international conference on soil mechanics and geotechnical engineering* (pp. 539-542). AA Balkema Publishers.

[7] Dai, F., Feng, Y., & Hough, R. (2014). Photogrammetric error sources and impacts on modeling and surveying in construction engineering applications. *Visualization in Engineering, 2*(1), 2.

[8] Habib, A. F., Ghanma, M. S., & Tait, M. (2004, July). Integration of LIDAR and photogrammetry for close range applications. In *Proceedings if the ISPRS XXth Conference*, Istanbul, Turkey B.

[9] Kadari, K. (2003). *Network designing of a digital close range photogrammetric system.* (Master's thesis, IIT Kanpur, India).

[10] Csanyi, N., & Toth, C. K. (2007). Improvement of lidar data accuracy using LiDAR-specific ground targets. *Photogrammetric Engineering & Remote Sensing*, *73*(4), 385-396.

[11] Hattori, S., Akimoto, K., Fraser, C., & Imoto, H. (2002). Automated procedures with coded targets in industrial vision metrology. *Photogrammetric engineering and remote sensing*, *68*(5), 441-446.

[12] Van Den Heuvel, F. A., Kroon, R. J. G. A., & Le Poole, R. S. (1993). Digital close-range photogrammetry using artificial targets. *International Archives of Photogrammetry and Remote Sensing*, *29*, 222-222.

[13] Li, L., & Liu, M. (2010). Research on decoding method of coded targets in close-range photogrammetry. *Journal of Computational Information Systems*, *6*(8), 2699-2705.

[14] Ahn, S. J., Rauh, W., & Kim, S. I. (2001). Circular coded target for automation of optical 3D-measurement and camera calibration. *International journal of pattern recognition and artificial intelligence*, *15*(06), 905-919.

[15] Mills, D., & Carty, G. (2005). Semi-automated crush determination using coded and non-coded targets with close-range photogrammetry. Retrieved from *http://www.PhotoModeler.com/applications/documents/MillsCodedTargetsCrush.pdf*.

[16] Chen, J., & Clarke, T. A. (1993). The automatic recognition, location and labelling of targets in digital photogrammetric engineering measurement. *International Archives of Photogrammetry and Remote Sensing*, *29*, 686-686.

[17] Shortis, M. R., Seager, J. W., Robson, S., & Harvey, E. S. (2003, January). Automatic recognition of coded targets based on a Hough transform and segment matching. *Electronic Imaging*, 202-208. International Society for Optics and Photonics.

[18] Jachimski, J., & Trocha, W. (1993). Determination of the Position of Crosses with Subpixel Accuracy on the Image Taken with the CCD Camera. *International Archives of Photogrammetry and Remote Sensing*, *29*, 391-391.

[19] West, G. A. W., & Clarke, T. A. (1990, August). A survey and examination of subpixel measurement techniques. *Close-Range Photogrammetry Meets Machine Vision, 1395,* 456-463.

[20] Wu, B., Hu, H., Zhu, Q., & Zhang, Y. (2013). A Flexible Method for Zoom Lens Calibration and Modeling Using a Planar Checkerboard. *Photogrammetric Engineering and Remote Sensing, 79*(6), 555-571.

[21] Pérez, M., Agüera, F., & Carvajal, F. (2011). Digital camera calibration using images taken from an unmanned aerial vehicle. *The International Archives of the Photogrammetry, Remote Sensing and Spatial Information Sciences, 38*(1), C22.

[22] Clarke, T. A. (1994, October). Analysis of the properties of targets used in digital close-range photogrammetric measurement. *Photonics for Industrial Applications*, 251-262. International Society for Optics and Photonics.

[23] Gonzales, R. C., & Woods, R. E. (2002). *Digital Image Processing, 6*, 681.

[24] Schenk, T. F. (1999). *Digital Photogrammetry: Backgrounds, Fundamentals, Automatic Orientation Procedures*. TerraScience.

[25] Chapra, S. C., & Canale, R. P. (2010). *Numerical methods for engineers*. New York: McGraw-Hill Higher Education.

[26] Li, Z., & Liu, M. (2010). Research on decoding method of coded targets in close-range photogrammetry. *Journal of Computational Information Systems, 6*(8), 2699-2705.

[27] Abdel-Aziz, Y. I., & Karara, H. M. (1971). Direct linear transformation from comparator coordinates into object-space coordinates in close-range photogrammetry. *Proceedings of the Symposium on Close-Range Photogrammetry*. Falls Church. VA: American Society of Photogrammetry.

[28] Wolf, P. R., & Ghilani, C. D. (1997). *Adjustment computations: statistics and least squares in surveying and GIS*. New York, NY, USA: John Wiley & Sons.

Biographies

SAGAR S. DESHPANDE is an assistant professor at Ferris State University, Department of Surveying Engineering. He earned his MTech degree in Civil Engineering from the Indian Institute of Technology Kanpur, India, in 2004 and MS degree in Geodetic Science from the Ohio State University in 2008. His current research interests include digital photogrammetry, remote sensing, and GIS. Professor Deshpande may be reached at sagardeshpande@ferris.edu